Supporting information for

Dantrolene rescues arrhythmogenic RYR2 defect in a patient-specific stem cell model of catecholaminergic polymorphic ventricular tachycardia

Christian B. Jung, Alessandra Moretti, Michael Mederos y Schnitzler, Laura Iop, Ursula Storch, Milena Bellin, Tatjana Dorn, Sandra Ruppenthal, Sarah Pfeiffer, Alexander Goedel, Ralf J. Dirschinger, Melchior Seyfarth, Jason T. Lam, Daniel Sinnecker, Thomas Gudermann, Peter Lipp, Karl-Ludwig Laugwitz

Content

Supplementary Materials and Methods

Localization of the S406L mutation in the context of the full-length ryanodine receptor

Recently, a crystal structure of the N-terminal 559 amino acids of ryanodine receptor 1 has been resolved (Tung *et al*, 2010), demonstrating that this disease hotspot region is composed of three individual domains, denoted as domains A, B and C. Analysis of several known disease-causing mutations localized in this region showed that all of them are either buried inside a domain or located at an interface between adjacent domains. This is consistent with a model postulating that opening of the channel leads to reorientation of the domains A, B and C in respect to each other and in respect to other domains of the ryanodine receptor. Mutations that destabilize the domain-domain interactions might, thus, destabilize the closed state of the receptor, thereby leading to an increased open probability (Tung *et al*, 2010).

Due to the high level of amino acid identity between the different ryanodine receptor isoforms, we were able to generate a structure of the N-terminal domain of human RYR2 (amino acids 12–543) by homology modeling (Roy *et al*, 2010). This structure was docked into the low-resolution cryo-EM-map of the ryanodine receptor using Sculptor software (Birmanns *et al*, 2011). Albeit a cryo-EM structure of RYR2 has been reported (Sharma *et al*, 1998), this map is not publicly available; since the differences between the reported RYR1 and RYR2 structures are only minor, we used the publicly available map of RYR1 (EMDB Entry EMD-5014) for these docking experiments. The Results of these docking studies (visualized by the UCSF Chimera package from the Resource for Biocomputing, Visualization, and Informatics at the University of California, San Francisco (supported by NIH P41 RR001081) (Pettersen *et al*, 2004) are shown in Supplementary Figure S3A and B. They show that the S406L mutation is located at an interface between domain B (which is part of domain 2 according to the nomenclature proposed by Radermacher et al. (Radermacher *et al*, 1994) and a domain of the ryanodine receptor (domain 1 according to the same nomenclature) which is not part of the crystal structure but forms a connection between the cytoplasmatic portion of the protein and the transmenbrane assembly. Replacement of the Serine at position 406 by the bulkier and hydrophobic Leucine might thus destabilize the interaction between these domains, destabilizing the closed state of the ryanodine receptor (see

Supplementary Figure S3C), in consistence with the model proposed by Tung et al. (Tung *et al*, 2010).

Birmanns S, Rusu M, Wriggers W (2011) Using Sculptor and Situs for simultaneous assembly of atomic components into low-resolution shapes. *J Struct Biol* **173:** 428-435

Pettersen EF, Goddard TD, Huang CC, Couch GS, Greenblatt DM, Meng EC, Ferrin TE (2004) UCSF Chimera--a visualization system for exploratory research and analysis. *Journal of computational chemistry* **25:** 1605-1612

Radermacher M, Rao V, Grassucci R, Frank J, Timerman AP, Fleischer S, Wagenknecht T (1994) Cryo-electron microscopy and three-dimensional reconstruction of the calcium release channel/ryanodine receptor from skeletal muscle. *The Journal of cell biology* **127:** 411-423

Roy A, Kucukural A, Zhang Y (2010) I-TASSER: a unified platform for automated protein structure and function prediction. *Nat Protoc* **5:** 725-738

Sharma MR, Penczek P, Grassucci R, Xin HB, Fleischer S, Wagenknecht T (1998) Cryoelectron microscopy and image analysis of the cardiac ryanodine receptor. *The Journal of biological chemistry* **273:** 18429-18434

Tung CC, Lobo PA, Kimlicka L, Van Petegem F (2010) The amino-terminal disease hotspot of ryanodine receptors forms a cytoplasmic vestibule. *Nature* **468:** 585-588

Supplementary Table S1.

Primers used for sequencing of the human RYR2 gene (exon 14) and qRT-PCR.

Gene	Use	Primer forward	Primer reverse
RYR2	Sequencing	TTGTTATGGCTCAGCTGTTTG	GCCTGGATGACAGTGTGAGA
ACTA2	qRT-PCR	GTGATCACCATCGGAAATGAA	TCATGATGCTGTTGTAGGTGGT
ADRB1	qRT-PCR	AAGAGAAAGGATGGAGGCAAA	GCCCTACACAAGGAAAGCAA
ADRB2	qRT-PCR	TGGTGATCATGGTCTTCGTCT	TCCACCTGGCTAAGGTTCTG
AFP	qRT-PCR	GTGCCAAGCTCAGGGTGTAG	CAGCCTCAAGTTGTTCCTCTG
CACNA1C	qRT-PCR	CAATCTCCGAAGAGGGGTTT	TCGCTTCAGACATTCCAGGT
CACNB2	qRT-PCR	GCAGCTGATAAACTGGCTCA	TCAAGCTGGTTCTCATCCAA
CALM1	qRT-PCR	ATCAGCTGACCGAAGAACAGA	CCTCATGACAGTTCCAAGTTCC
CALR	qRT-PCR	GCATACGCTGAGGAGTTTGG	CTGCTCCTCGTCCTGTTTGT
CASQ2	qRT-PCR	CCGGGACAATACTGACAACC	CTTCTCCCAGTAGGCAACGA
CD31	qRT-PCR	ATGCCGTGGAAAGCAGATAC	CTGTTCTTCTCGGAACATGGA
CLCN4	qRT-PCR	TCTTCAGGAACTGGTGCAGAC	TGATGACCACCAATGACACC
c-MYC endogenous	qRT-PCR	AGAAATGTCCTGAGCAATCACC	AAGGTTGTGAGGTTGCATTTGA
c-MYC transgene	qRT-PCR	GGAAACGACGAGAACAGTTGA	CCCTTTTTCTGGAGACTAAATAAA*
DES	qRT-PCR	GTGAAGATGGCCCTGGATGT	TGGTTTCTCGGAAGTTGAGG
FKBP1B	qRT-PCR	CTCTGCCCAAGTTGCTCTGT	TCTGCAACCGAAGTTTCCTC
GABRR2	qRT-PCR	CTGTGCCTGCCAGAGTTTCA	ACGGCCTTGACGTAGGAGA
GAPDH	qRT-PCR	TCCTCTGACTTCAACAGCGA	GGGTCTTACTCCTTGGAGGC
HCN4	qRT-PCR	CAATGAGGTGCTGGAGGAGT	GGTCGTGCTGGACTTTGTG
KCNH2 (1a)	qRT-PCR	GGCTCATGACACCAACCAC	TTCAGGCGGAAGGTCTTG
KCNH2 (1b)	qRT-PCR	ACGCTTACTGCCAGGGTGAC	GCCGACTGGCAACCAGAG
JCTN	qRT-PCR	ACAAAGCATGGAGGACACAAG	GCAATGCAATCACCATAAACC
KCNA4	qRT-PCR	TCATTGCTCTGACCTGATGC	TCACTCAGCTCCCTCAGGAT
KCNJ11	qRT-PCR	GGACGGACGTTACTCTGTGG	GTAGGCTGTGGTCCTCATCAA
KCNJ2	qRT-PCR	GTGTCCGAGGTCAACAGCTT	GGTTGTCTGGGTCTCAATGG
KCNK3	qRT-PCR	CAACCTCCCTTCGTGTTGTT	TGCTGGGTTTCCACTTTCTC
KCNQ1	qRT-PCR	CGCCTGAACCGAGTAGAAGA	TGAAGCATGTCGGTGATGAG
KLF4 endogenous	qRT-PCR	ATAGCCTAAATGATGGTGCTTGG	AACTTTGGCTTCCTTGTTTGG
KLF4 transgene	qRT-PCR	CCACCTCGCCTTACACATGA	CCCTTTTTCTGGAGACTAAATAAA*
KRT14	qRT-PCR	CACCTCTCCTCCTCCCAGTT	ATGACCTTGGTGCGGATTT
MYL2	qRT-PCR	TACGTTCGGGAAATGCTGAC	TTCTCCGTGGGTGATGATG
MYL7	qRT-PCR	CCGTCTTCCTCACGCTCTT	TGAACTCATCCTTGTTCACCAC
NANOG	qRT-PCR	TGCAAGAACTCTCCAACATCCT	ATTGCTATTCTTCGGCCAGTT
NCAM1	qRT-PCR	CAGATGGGAGAGGATGGAAA	CAGACGGGAGCCTGATCTCT
OCT4 endogenous	qRT-PCR	GACAGGGGGAGGGGAGGAGCTAGG*	CTTCCCTCCAACCAGTTGCCCCAAAC*
OCT4 transgene	qRT-PCR	GCTCTCCCATGCATTCAAAC	TTATCGTCGACCACTGTGCTGCTG*
PDX1	qRT-PCR	GATGAAGTCTACCAAAGCTCACG	GTTCAACATGACAGCCAGCTC
PLN	qRT-PCR	TCCCATAAACTGGGTGACAGA	TGATACCAGCAGGACAGGAAG
PPA1	qRT-PCR	ACCACCACCCTGTGAATCTG	TTTTCTGGTGATGGAACCACTT
PPP2R4	qRT-PCR	CCTTCCTGGTCCAAAGTGAA	GTGCTGGATCACAGGGAACT
REX1	qRT-PCR	ACCAGCACACTAGGCAAACC	TTCTGTTCACACAGGCTCCA
RYR2	qRT-PCR	GCTATTCTGCACACGGTCATT	ATTTCCGTGCCACTTCCTTT
SCL	qRT-PCR	CCAACAATCGAGTGAAGAGGA	CCGGCTGTTGGTGAAGATAC
SCNA5	qRT-PCR	GAGCTCTGTCACGATTTGAGG	GAAGATGAGGCAGACGAGGA
ATP2A2a (SERCA2a)	qRT-PCR	TCATGGATGAGACGCTCAAGT	ACCGAACACCCTTACATTTCTG
SLC8A1	qRT-PCR	GAGACCTGGCTTCCCACTTT	ATTCCCAGGAAGACATTCACC
SOX2 endogenous	qRT-PCR	GGGAAATGGGAGGGGTGCAAAAGAGG*	TTGCGTGAGTGTGGATGGGATTGGTG*

SOX2 transgene	qRT-PCR	GGCCATTAACGGCACACTG	CCCTTTTTCTGGAGACTAAATAAA*
SOX7	qRT-PCR	TGAACGCCTTCATGGTTTG	AGCGCCTTCCACGACTTT
TDGF1	qRT-PCR	CCCAAGAAGTGTTCCCTGTG	ACGTGCAGACGGTGGTAGTT
TH	qRT-PCR	TGTACTGGTTCACGGTGGAGT	TCTCAGGCTCCTCAGACAGG
TNNT2	qRT-PCR	AGCATCTATAACTTGGAGGCAGAG	TGGAGACTTTCTGGTTATCGTTG
TRDN	qRT-PCR	GTGTCTCCCACAAAGCAGAAA	GGTCTGCAGGAGTGAAAGGA

* Takahashi K, Tanabe K, Ohnuki M, Narita M, Ichisaka T, Tomoda K, Yamanaka S (2007) Induction of pluripotent stem cells from adult human fibroblasts by defined factors. *Cell* **131:** 861-872

Supplementary Figures

Supplementary Figure S1. Expression profile and pluripotency potential of generated iPSC lines by real time quantitative PCR analysis.

Supplementary Figure S2. Intracellular Ca^{2+} recordings in iPSC-derived cardiomyocytes.

Supplementary Figure S3. Percentage of cells with normal and aberrant Ca^{2+} cycling in electrically stimulated myocytes from different control and CPVT-iPSC clones.

Supplementary Figure S4. Measurements of luminal SR Ca^{2+} by the mean of a low-affinity Ca^{2+} indicator, Fluo-5N AM, in iPSC-derived myocytes.

Supplementary Figure S5. Modeling of the location and schematic representation of the proposed mechanism of action of the disease-causing mutation.

Supplementary Figure S6. Dantrolene corrects the arrhythmogenic phenotype in atrial-like CPVT-iPSC-derived myocytes.

Supplementary Movie Legends

Supplementary Movie S1. Ca^{2+} sparks in a representative control iPSC-derived myocyte under basal conditions. Synced image sequences of pseudo-colored images of fluo-4-AM loaded control myocyte (top), corresponding 3D surface plot (left), and Ca^{2+} traces of corresponding regions of interest under basal conditions.

Supplementary Movie S2. Ca^{2+} sparks in a representative CPVT iPSC-derived myocyte under basal conditions. Synced image sequences of pseudo-colored images of fluo-4-AM loaded control myocyte (top), corresponding 3D surface plot (left), and Ca^{2+} traces of corresponding regions of interest under basal conditions.

Supplementary Movie S3. Ca^{2+} sparks in a representative control iPSC-derived myocyte under 1 μM isoproterenol. Synced image sequences of pseudo-colored images of fluo-4-AM loaded control myocyte (top), corresponding 3D surface plot (left), and Ca^{2+} traces of corresponding regions of interest under isoproterenol stimulation.

Supplementary Movie S4. Ca^{2+} sparks in a representative CPVT iPSC-derived myocyte under 1 μM isoproterenol. Synced image sequences of pseudo-colored images of fluo-4-AM loaded control myocyte (top), corresponding 3D surface plot (left), and Ca^{2+} traces of corresponding regions of interest under isoproterenol stimulation.

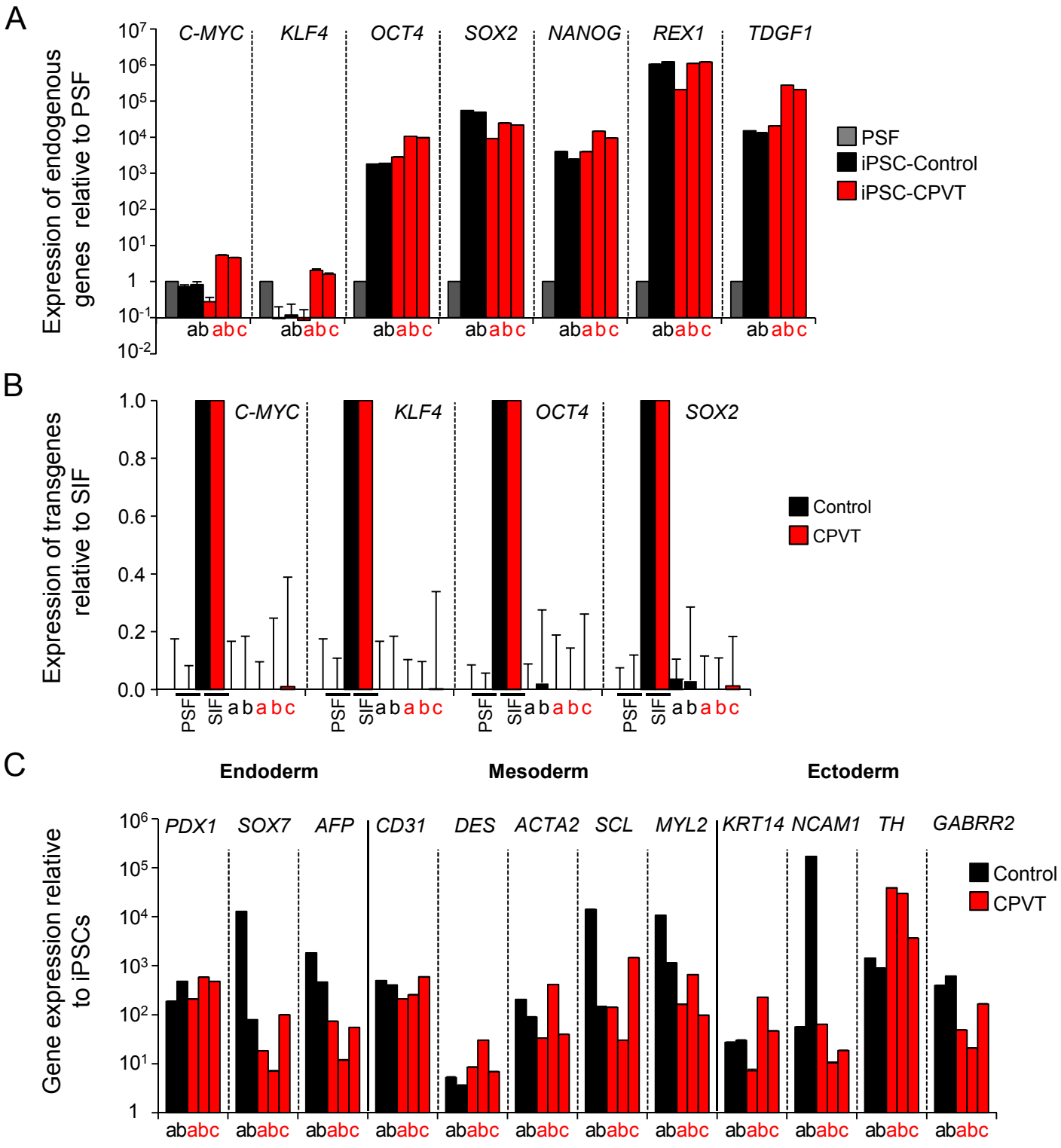

Supplementary Figure S1. Expression profile and pluripotency potential of generated iPSC lines by real time quantitative PCR analysis. Different clones from control (black) and CPVT (red) cells are indicated with a, b, and c. (**A**) Re-expression of endogenous genes associated with pluripotency. Expression values are relative to corresponding primary skin fibroblasts (PSF). (**B**) Silencing of the four transgenes used for the reprogramming. Expression levels are relative to corresponding skin fibroblasts after retroviral infection (SIF). (**C**) Up-regulation of lineage markers representative of the three embryonic germ layers in iPSC-derived embryoid bodies at day 21 of differentiation. Expression levels are relative to corresponding undifferentiated iPSC clones. All expression values are normalized to *GAPDH* and are presented as mean ± SEM, n=3.

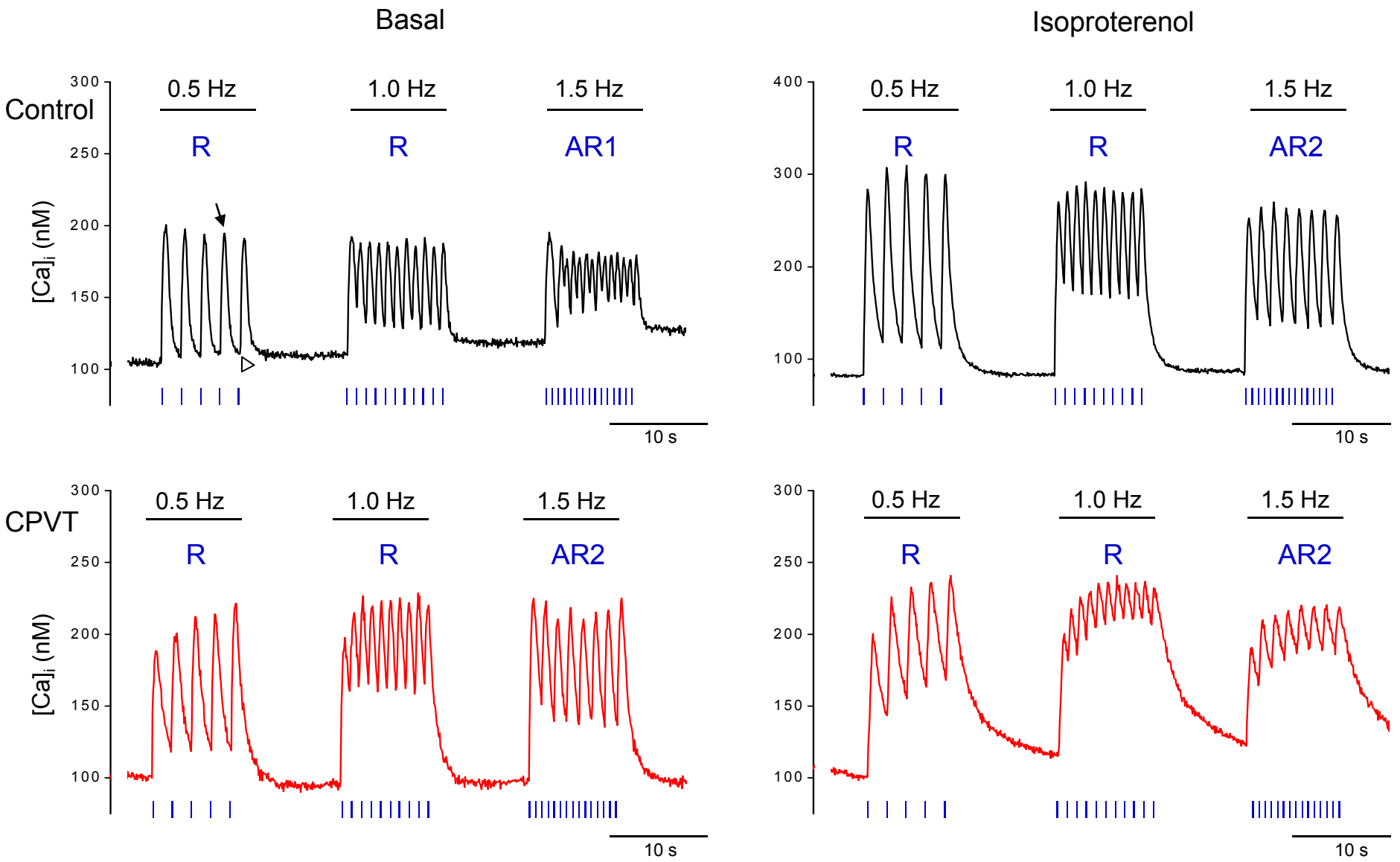

Supplementary Figure S2. Intracellular Ca^{2+} recordings in iPSC-derived cardiomyocytes. Representative recordings of Ca^{2+} transients in control (black, top) and CPVT (red, bottom) myocytes loaded with fura-2-AM and electrically stimulated at 0.5, 1, and 1.5 Hz in absence (left) and in presence (right) of 10 μM isoproterenol. Blue lines indicate electric stimuli. R, regular Ca^{2+} cycling; AR1, Ca^{2+} alternans; AR2, Ca^{2+} transient fusion. Arrow and arrowhead indicate where systolic and diastolic Ca^{2+} values where measured, respectively. Alternatively, stimulation protocols using only one pacing frequency were applied.

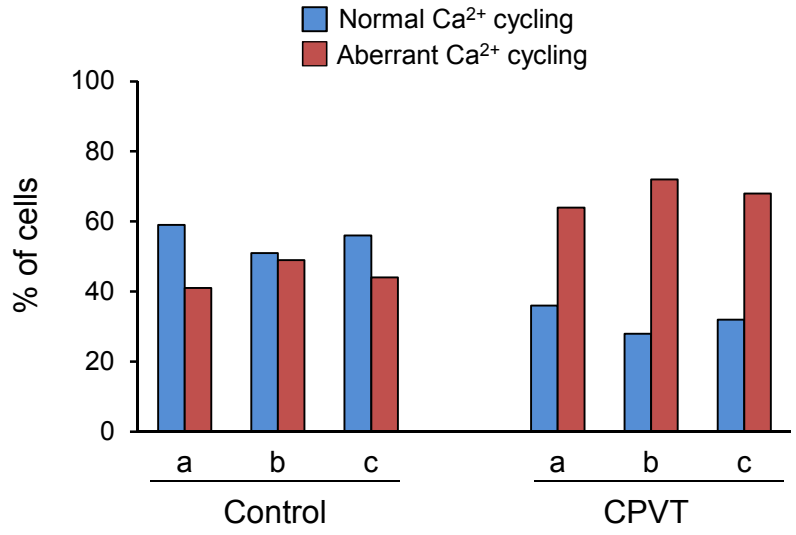

Supplementary Figure S3. Percentage of cells with normal and aberrant Ca^{2+} cycling in electrically stimulated myocytes from different control and CPVT-iPSC clones. Three iPSC clones (a, b, and c) derived from the healthy control individual and the CPVT patient are compared. Between 11 and 22 cells were analyzed per clone. Percentage of cells with aberrant Ca^{2+} cycling at 1 Hz stimulation is similar among clones within the same group.

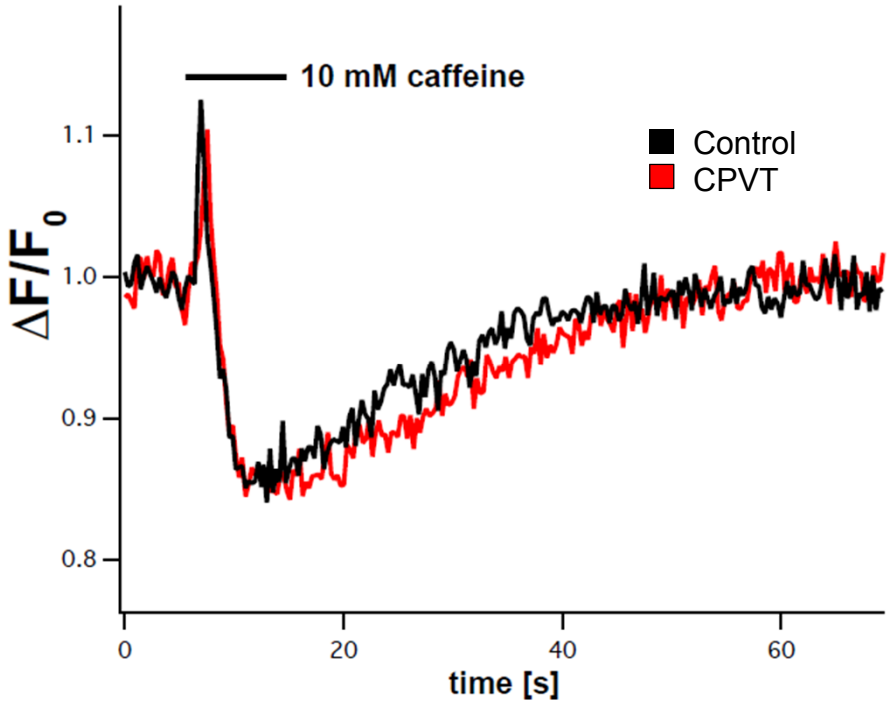

Supplementary Figure S4. Measurements of luminal SR Ca^{2+} by the mean of a low-affinity Ca^{2+} indicator, Fluo-5N, in iPSC-derived myocytes. Averaged trace illustrating relative changes of the SR Ca^{2+} concentration in control (n=9) and CPVT (n=12) myocytes after application of 10 mM caffeine. In both control and CPVT cells caffeine resulted in a similar unloading amplitude in SR Ca^{2+}. Before the experiment, cells were loaded for 2 h at 37 C with a final concentration of 15 μM Fluo-5N (AM version), followed by a 1.5 h washing step allowing for the de-esterification of the dye and the removal of Fluo-5N from the cytosol.

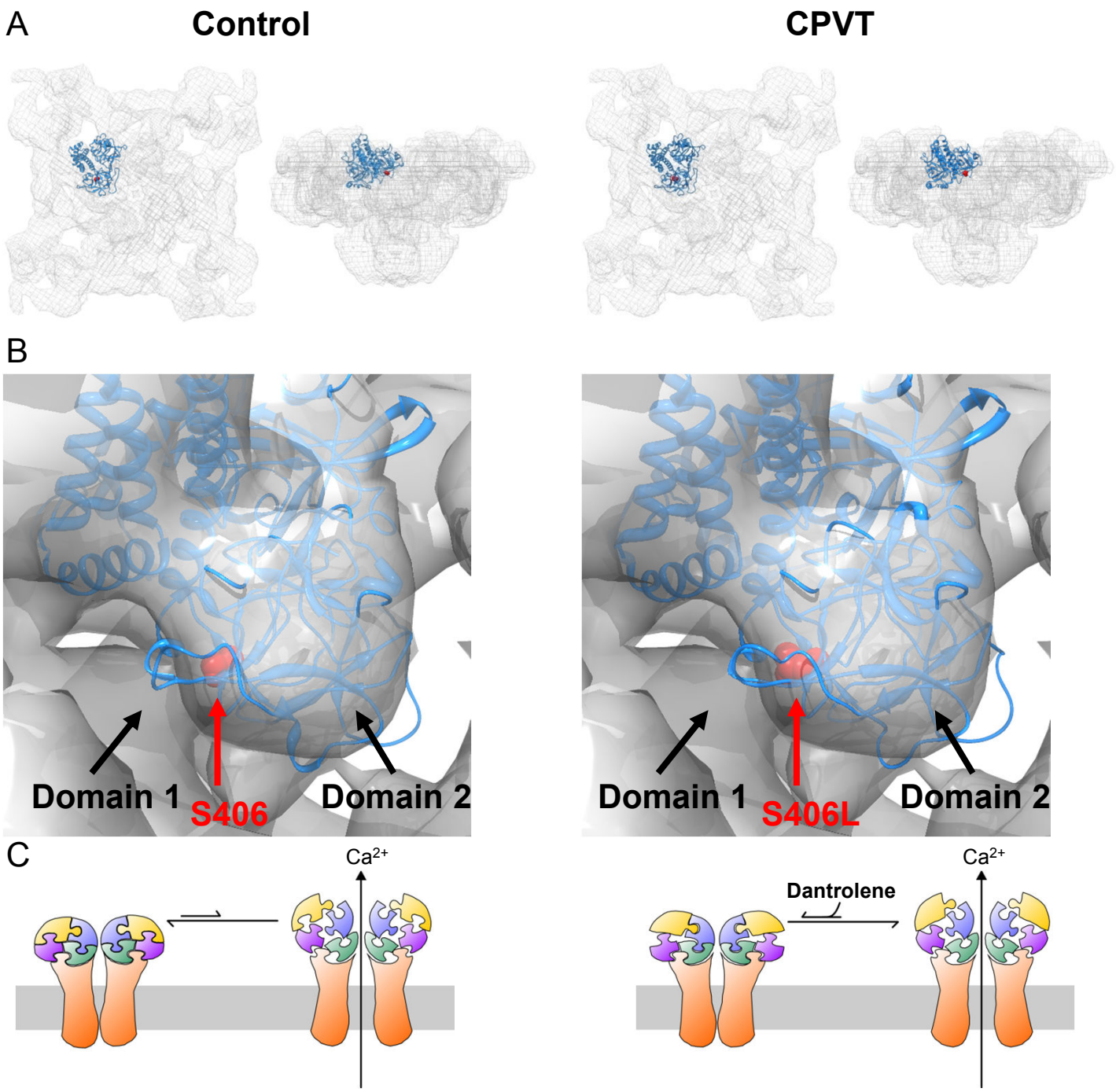

Supplementary Figure S5. Modeling of the location and schematic representation of the proposed mechanism of action of the disease-causing mutation. The left panel shows the situation in control subjects, the right panel that in CPVT patients. (**A**) The homology-modeled structure of the N-terminal 559 amino acids of human wild type and S406L-mutated RYR2 (blue ribbons, Serine 406/Leucine 406 is depicted in red) is shown docked into the cryo-electron microscopy density map of ryanodine receptor (grey structure). Shown are a view from the cytosol (left image) and a side view (right image). (**B**) A close-up view of the localization of Serine 406/Leucine 406 in the context of the adjacent protein domains is shown. (**C**) A cartoon depicting the proposed mechanism of action of the CPVT-causing S406L mutation is shown. The multiple domains of RYR2 that interact with each other and thereby stabilize the closed state of the ion channel are depicted as pieces of a jigsaw puzzle. In the CPVT patient, the S406L mutation interferes with normal domain-domain interaction, leading to an increased probability of domain unzipping. This can be reversed by dantrolene, which stabilizes the domain-domain interactions.

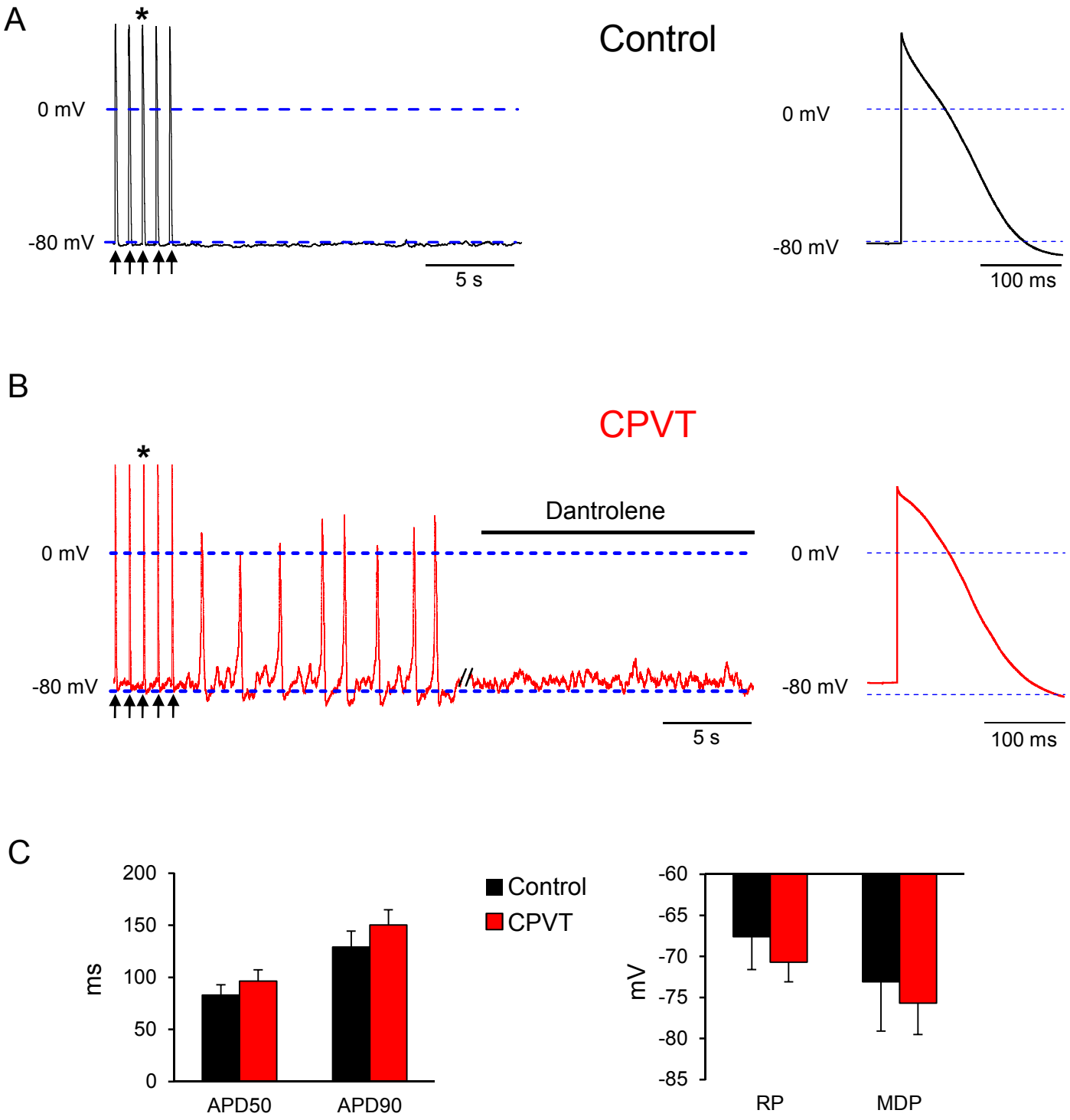

Supplementary Figure S6. Dantrolene corrects the arrhythmogenic phenotype in atrial-like CPVT-iPSC-derived myocytes. (**A, B**) Representative electrically evoked action potentials from a control (**A**) and CPVT (**B**) atrial-like myocyte. Black arrows indicate the last 5 paced action potentials at 1 Hz stimulation. Right, action potentials shown at an expanded time scale taken from the region indicated on the left (*). Superfusion with 10 μM dantrolene completely abolished DADs and TA in CPVT cells. (**C**) Bar graphs of the averaged action potential duration at 50% (APD50) and 90% (APD90) repolarization (left), the maximum diastolic potential (MDP), and the resting potential (RP) (right) during stimulation at 1 Hz.